Cellulose (2018) 25:1795–1807
https://doi.org/10.1007/s10570-018-1703-9

ORIGINAL PAPER

Cyclic tensile properties of the polylactide nanocomposite foams containing cellulose nanocrystals

Yaxin Qiu · Qiaolian Lv · Defeng Wu · Wenyuan Xie · Sheng Peng · Ruyue Lan · Hui Xie

Received: 13 November 2017 / Accepted: 5 February 2018 / Published online: 7 February 2018

Abstract Cellulose nanocrystal (CNC) filled polylactide (PLA) nanocomposites are of interest because both the filler particles and matrix polymer are biodegradable. Foaming with high pressure inert gas is a promising way to open potential applications of this kind of green nanocomposites as lightweight materials. To establish the structure–property relations of this kind of foams is hence of great significance. In this work, PLA/CNC nanocomposites containing three types of CNC particles, including pristine CNC and acetylated ones with lower and moderate degrees of substitution, were foamed using CO_2 as the blowing agent for the studies mentioned above. The results show that the presence of all three kinds of CNC particles has large influence on cellular structure and cell morphology, and as a result, affects final mechanical properties of foams. The tensile cycle tests were then performed as an efficient tool to further figure out clear information on the contributions of reinforcement of filler and altered cell structure to the plasticity and elasticity of foams. The obtained results provide useful information on the optimization of cell structure and mechanical properties of PLA foams using small amounts of CNC particles through controlling their surface properties.

Keywords Cellulose nanocrystal · Polylactide · Nanocomposites · Foams · Cyclic tensile properties

Y. Qiu · Q. Lv · D. Wu (✉) · W. Xie · S. Peng · R. Lan · H. Xie
School of Chemistry and Chemical Engineering, Yangzhou University, Yangzhou 225002, Jiangsu, People's Republic of China
e-mail: dfwu@yzu.edu.cn

Y. Qiu · D. Wu · W. Xie
Provincial Key Laboratories of Environmental Engineering and Materials, Yangzhou 225002, Jiangsu, People's Republic of China

Introduction

Cellulose nanocrystal (CNC) filled polylactide (PLA) nanocomposites have attracted much interest from both the industrial and academic fields in recent years (Raquez et al. 2013; Miao and Hamad 2013). The main reason is because both matrix polymer and filler particle are bio-originated and biodegradable, and therefore this kind of nanocomposites is fully green. On the other hand, CNC particles have high elastic modulus and strength, as well as aspect ratio, and their reinforcement is able to open potential applications of PLA. Thus, as an interesting green nanocomposite system, PLA/CNC has been extensively studied so far. The reported studies mainly focused on four aspects: (1) surface modification of CNC to improve its compatibility with PLA (Dhar et al. 2016; Dong et al. 2017; Fortunati et al. 2012a; Pracella et al. 2014; Xu et al. 2016; Spinella et al. 2015; Lin et al. 2011); (2) establishing the relationship between properties and

different structures of PLA/CNC nanocomposites (Xu et al. 2016; Spinella et al. 2015; Lin et al. 2011; Xu et al. 2017a, b; Fortunati et al. 2015; Khoshkava and Kamal 2014; Zhao et al. 2016; Fortunati et al. 2014; Shi et al. 2012; Herrera et al. 2016; Parize et al. 2017; Luzi et al. 2015); (3) introducing the third components (such as polymers, nanoparticles, etc.) to control the phase structure or to multi-functionalized PLA/CNC nanocomposites (Arrieta et al. 2015; Haque et al. 2017; Cacciotti et al. 2014; Yu et al. 2016; Fortunati et al. 2012b; Arrieta et al. 2014; Bitinis et al. 2013a, 2013b; Luzi et al. 2016; Pal et al. 2017; Fortunati et al. 2013); (4) exploring potential applications of PLA/CNC nanocomposites in food packaging and tissue engineering as well as other bio-related fields (Pal et al. 2017; Fortunati et al. 2013; Salmieri et al. 2014; Zhou et al. 2013; Zhang et al. 2015; Dhar et al. 2017; Alvarado et al. 2018).

Foaming has been an interesting topic on the studies of PLA and its nanocomposites in the past decades because lightweight materials can further extend applications of PLA (Nofar and Park 2014). The conventional polymeric foams like polypropylene (PP), polyurethane (PU), polystyrene (PS), etc., are major market players nowadays, which are non-degradable, however. Therefore, PLA foams have potential to compete with those conventional petroleum based foams, especially in the application fields where degradability is a major area of concern. Two routes are commonly employed to prepare PLA foams. One is the continuous process through the extrusion foaming or injection or beads molding one, which has already been industrialized. Another is the batch foaming using inert gas as the blowing agent, which is often performed for academic research. For the continuous process, the use of chain extender is necessary to increase the melt strength and elasticity of PLA to widen its foaming window and to improve cell structure. The batch foaming in solid state is relatively green and the microcellular structure of as-obtained PLA foams is controllable. More interestingly, the reported studies revealed that the addition of small amount of nanoparticles could be an effective way to further control expansion ratio and cell density of PLA foams because the presence of those particles not only serves as nucleation agents, but also has strong influence on the gas diffusivity and bubble growth (Nofar and Park 2014; Zhang et al. 2014; Liao et al. 2010; Fang et al. 2013; Xu et al. 2014). This provides a promising approach to design or to control cell structure of PLA foams, or to fabricate functionalized PLA nanocomposite green foams. Thus, solid-state foaming of the PLA nanocomposites filled with a variety of particles has been explored in detail (Keshtkar et al. 2014; Ji et al. 2013; Kang et al. 2009; Ema et al. 2006).

The effect of cellulose nanoparticles on the solid state foaming of PLA has also been studied preliminarily (Dlouhá et al. 2012; Cho et al. 2012). Dlouhá et al. (2012) reported that the introduction of cellulose nanofibres (CNFs) significantly improved the cell morphology of PLA foams. The reduced cell size and increased cell density were closely related to the amount of CNFs and their surface acetylation. Cho et al. (2012) also prepared PLA/CNF foams by the supercritical CO_2 foaming and found that the cell size reduced monotonously with increasing CNF loadings. However, the foam density reduced at lower CNF loadings but increased at higher loading levels. They attributed this to a synergistic effect of rheological properties and the degrees of crystallinity of matrix. As for the PLA/CNC composites, the work on its physical foaming is very limited. Borkotoky et al. (2017) reported a similar change trends of cell size and morphology in the PLA/CNC composite foams with those found in the supercritical fluid foamed PLA/CNF systems. But their composite foams were prepared by casting and leaching method.

Clearly, there is still large space to be filled around the foaming study of PLA/CNC systems. In the previous work (Xu et al. 2016, 2017b), we studied the phase interactions of the PLA nanocomposites containing the acetylated CNC particles with various surface substitution levels. The results revealed that the acetylated CNC could disperse better than the pristine one, with decreased aggregation level and increased effective filling volume, because of improved interfacial interactions due to hydrogen bonding. This favors improvement of final mechanical strength of composites. The presence of CNC particles, whether the pristine or the acetylated ones, however, had nearly no influence on the amorphous morphology of matrix PLA. For the foaming of those composite systems, there are hence many interesting questions arisen. Do the CNC particles with various modification levels have different influence on the cell structure of PLA foams? If yes, what is the relations between final properties of foams and their different-

level structures (for instance, cell size and morphology, and cell wall surface and thickness, etc.). These issues are worthy of deep exploration. Thus, in this work, PLA/CNC composite foams were prepared by batch foaming using CO_2 as the blowing agent for the studies mentioned above. Three types of CNC particles, including the pristine CNC and the acetylated one with lower and moderate degrees of substitution, were used. The cell structures of nanocomposite foams was then studied, aiming at disclosing multiple roles that those CNC particles played during solid state foaming of PLA. The cyclic tensile behavior of those composite foams was further evaluated with the objective to reveal the effect of CNC particles on the microcellular structures and mechanical properties of foams. This work provides a possibility to control cellular structures of green PLA foams using the CNC particles with various surface properties.

Experimental

Material preparation

Polylactide (2002D) is a commercial product purchased from Nature Works Co. Ltd., USA. It has the number average molecular weight of about 80,000 g mol^{-1}, with the density of 1.24 g cm^{-3} (ASTM D792). The microcrystalline cellulose (MCC) used for the preparation of CNC was purchased from Sinopharm Chemical Reagent Co. Ltd., P. R. China. It is a white powder sample (10–20 μm diameter and 20–100 μm length), with the degree of polymerization (DP) of 210–240.

CNC particles were produced by acidic hydrolysis of MCC as described previously (Chen et al. 2015). The average diameter and length of as-prepared CNC particles are about 10–20 and 200–300 nm, respectively (Xu et al. 2016). The acetylation of CNC and the following preparation of PLA/CNC composites followed a continuous route developed in the previous work (Xu et al. 2016; Lv et al. 2017), namely the solvent-assisted centrifugation method without any freeze drying step. The composite film (about 0.2 mm thickness) were then prepared by solution casting, followed by vacuum-drying to constant mass weight. To avoid any effect of residual solvent on the following foaming step, the film was cut into small pieces and then experienced melt extrusion using a Haake mini-lab (180 °C, 3 min). Finally, the sheet samples (about 1 mm thickness) used for the following foaming were obtained by compression molding (180 °C, 15 MPa). The filler contents (weight loadings) were 3 wt% for all samples. Three kinds of CNC particles, namely pristine CNC, and acetylated CNCs (*a*CNC) with lower degree of substitution (DS, 0.58) and moderate DS (1.26) were used here (as excessive acetylation (DS > 2) could destroy crystalline structure of CNC particles, leading to decreased aspect ratio and rigidity (Xu et al. 2017b). After acetylation with lower or moderate DSs, CNC particles kept their original rod-like structure (10–20 nm diameter and 200–250 nm length) well (Xu et al. 2017b). The DSs were evaluated by a method developed by Xin et al. (2011) based on the ^{1}H nuclear magnetic resonance (^{1}H NMR) spectroscopy analysis on the ratios of the integration value of $–CH_3$ to that of cellulose backbone. Details could be found in the previous work (Xu et al. 2016, 2017b). Hereafter the composite samples with CNC particles and *a*CNC ones are referred as to PLA–CNC and PLA–*a*CNC(L), as well as PLA–*a*CNC(M), where L and M denote the lower DS and moderate one of *a*CNC, respectively.

The batch foaming assisted with high pressure CO_2 were used to prepare PLA/CNC composite foams. The supercritical point for CO_2 fluid is about 7.39 MPa (31.3 °C). For some amorphous polymers, however, 3–6 MPa (0 °C) saturated pressure are more appropriate for their batch foaming (Zhang et al. 2014) because in this case good cellular structure can be achieved. For the amorphous PLA used in this work, foaming with a high-level pressure (> 5–6 MPa) might result in the formation of uneven cell structure or layered cellular morphology (Liao et al. 2010; Wu et al. 2015), or even leads to the formation of cell opening structure in the presence of filler particles, with rather poor cell wall structure (Ji et al. 2013; Matuana and Faruk 2010). Therefore, the common foaming conditions (saturated pressure 5 MPa, and temperature 0 °C-room temperature), which were widely used for the academic studies of batch foaming of filled PLA composite systems (Fang et al. 2013; Xu et al. 2014; Wu et al. 2015; Wang et al. 2012; Matuana 2008), were employed here to prepare the PLA/CNC composite foams also. Firstly, the sheet samples (about 3 cm × 6 cm × 1 mm) were enclosed in a high-pressure vessel connected with a CO_2 cylinder, and saturated with CO_2 at 0 °C and 5 MPa for 12 h.

Then, CO_2 was quickly released from the vessel (from 5 to 0.1 MPa within 3 min) and the samples were removed and immediately immersed into a water bath, foamed for 30 s at 60 °C. Finally, the foamed samples were quenched in cold water (15 °C), followed by a vacuum-drying to remove traces of water. All samples had the same foaming histories.

Cell morphology characterizations

The cell structure of foams is observed by an S-4800 scanning electron microscopy (SEM, Hitachi, Japan) at the 15 kV accelerating voltage. The sheet samples were frozen in liquid nitrogen and fractured. The fractured surface was coated with gold by an SPI sputter coater for the observation. The cell density (N_c) is defined by Ema et al. (2006)

$$N_c = 10^4 \frac{3[1 - \rho_f/\rho_0]}{4\pi d^3} \quad (1)$$

where d is number average cell size, ρ_0 and ρ_f pre-foamed mass density and post-foamed one. The average wall thickness (δ) can then be evaluated through mass density ratio (Nam et al. 2002)

$$\delta = d(1/\sqrt{1 - \rho_f/\rho_0} - 1) \quad (2)$$

and the mass densities of the samples before and after foaming were measured by the water displacement method based on ISO 1183-1987.

Mechanical property tests

The tensile behavior of foams was determined using an Instron Mechanical Tester at a crosshead speed of 1 mm min^{-1} at 25 °C. The strength and modulus values reported here are average ones of six parallel tests. The dumbbell-shaped specimens (about 1 mm thick, 2 mm wide and 15 mm neck length) used for the tensile tests were cut from foam sheets. The step cycle tensile tests were performed with the stretching rate of 1 mm s^{-1}. As the sample reached the target strain/stress, the crosshead direction was reversed up to the zero strain/stress at the same crosshead speed. The sample was then stretched again until the strain/stress reached next level. For the strain-controlled step cycle tensile, the test was performed procedurally (2, 4, 6,8 mm…) till the sample was broken. For the stress-controlled procedure, the step value was set as 1.5 MPa (1.5, 3.0, and 4.5 MPa…, up to the broken level).

Results and discussion

Cellular morphology of PLA and its nanocomposite foams

Figure 1 shows SEM images of PLA and its nanocomposite foams. PLA foam has good microcellular morphology and smooth wall structure (Fig. 1a, a′) at current foaming conditions, with the average cell size of 35 μm. It is clear that the presence of CNC particles, including both the pristine and acetylated ones, leads to an increased expansion ratios ($R_v = \rho_0/\rho_f$) of foamed systems, and hence reduces cell size and increases cell density evidently at current loading levels (3 wt%) (Fig. 1b–d, b′–d′). Besides, the nanocomposite foams present rough wall surface as compared with the neat PLA one. These indicates that the presence of CNC particles has large influence on the microcellular structures of PLA foams.

It is accepted that a physical foaming process has three stages, namely the nucleation, bubble growth, and stabilization of cellular structure. A small amount of nanoparticles may serve as preferential nucleation sites with a lower energy barrier of nucleation, facilitating cell nucleation process (Keshtkar et al. 2014; Ema et al. 2006; Dlouhá et al. 2012; Fang et al. 2013; Xu et al. 2014). Therefore, it is reasonable to propose that CNC particles have good nucleation effect on the physical foaming of PLA. It should be addressed here that both the neat PLA and its nanocomposites are amorphous (Xu et al. 2017a) (there are no thermal events on the DSC curves in the cooling process and no diffraction peaks on XRD patterns as quenched from molten state for both the pristine CNC and *a*CNC filled PLA nanocomposites). In this case the effect of PLA bulk crystallization (for instance, the alteration of degrees of bulk crystallinity) can be ignored. On the other hand, the dispersed CNC particles can act as the role of physical barriers (namely retarding the coalescence of two adjacent bubbles) to stabilize the nucleated bubbles. Besides, in the previous work (Xu et al. 2016), it was found that the presence of CNC particles (including both the pristine CNC and *a*CNC) increases the melt viscosities and moduli, and the moduli in both glassy and rubbery

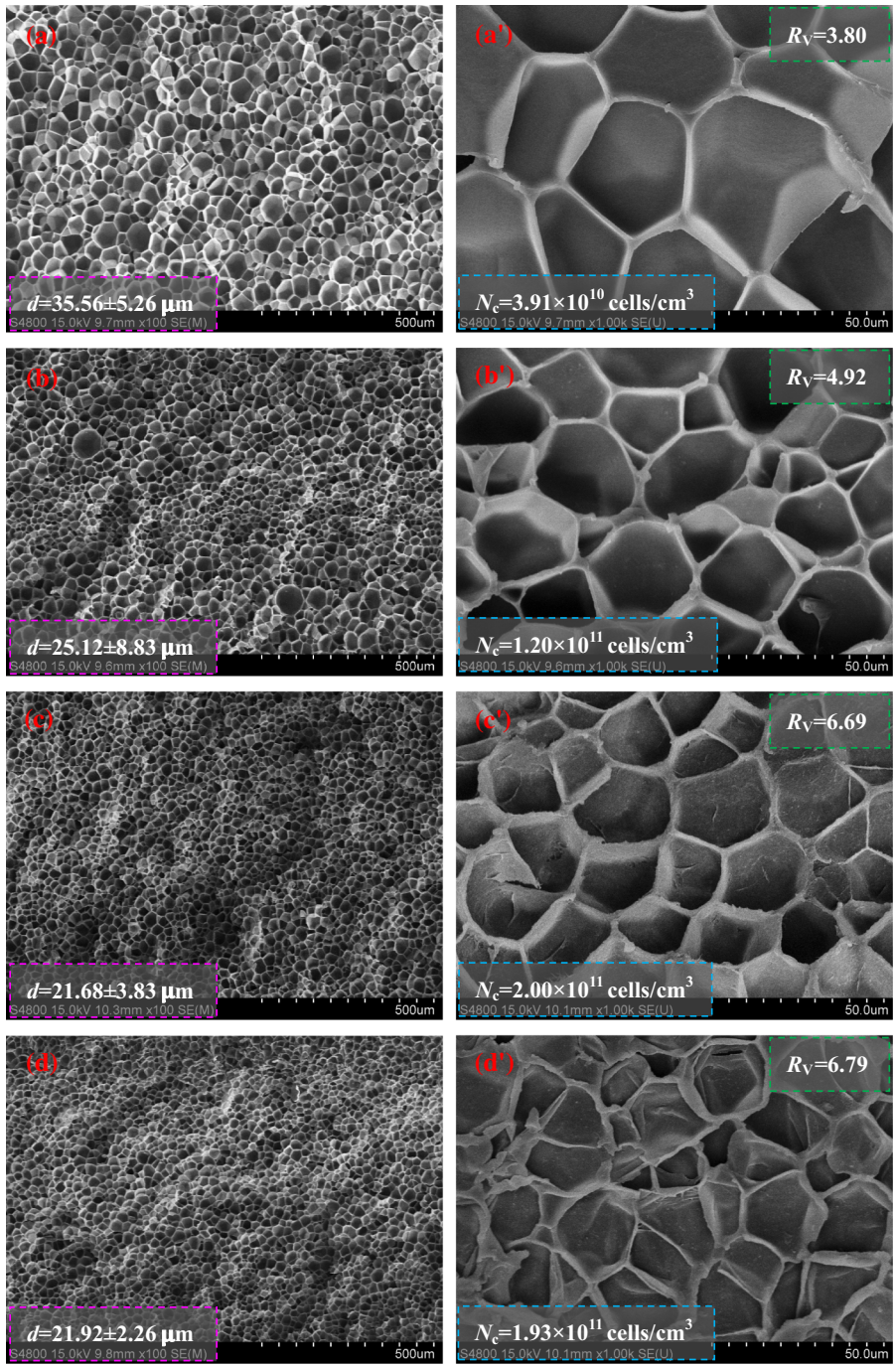

Fig. 1 SEM images for **a**, **a′** PLA, **b**, **b′** PLA–CNC, **c**, **c′** PLA-*a*CNC(L) and **d**, **d′** PLA-*a*CNC(M) foams with the scale bars of 500 μm (**a**–**d**) and 50 μm (**a′**–**d′**)

state. This favors slowing down the bubble growth rates (Li et al. 2017). Therefore, the decrease in cell size and increase in cell density of PLA foams in the presence of CNC particles are attributed to the synergistic effects caused by nucleation and barrier role of CNC particles, as well as increased system rigidity.

It is notable that the nanocomposite foams containing *a*CNC have lower cell size and higher cell density evidently than the one with pristine CNC (Fig. 1b–d, b′–d′) at the same loadings (3 wt%). This is mainly attributed to the difference in dispersion state of filler particles and their interactions with matrix PLA caused by different surface properties between pristine CNC and *a*CNC, which was studied in the previous work in detail (Xu et al. 2017b). The nucleating efficiency of the nanoparticles is generally compromised by their aggregation or their high interactions with the polymer matrix (Ema et al. 2006; Dlouhá et al. 2012). Better dispersion of nanoparticles can provide higher amounts of nucleating sites, which needs the improvement of phase adhesion. However, the improved polymer-particle compatibility is unfavorable for nucleation because a weak phase interface is commonly preferred for heterogeneous nucleation during physical foaming (Dlouhá et al. 2012; Wu et al. 2015). As discussed in the previous work (Xu et al. 2016), acetylation could improve the interfacial interactions between PLA and CNC particles (confirmed by appearance of new C1*s* signal on XPS spectra, which was assigned to hydrogen-bonded carbon atom), resulting in better dispersion of *a*CNC in PLA than that of pristine CNC. The decreased aggregation level and increased effective filling volume of filler particles [indicated by decreased rheological percolation thresholds of the *a*CNC filled PLA systems (Xu et al. 2016)] indicates that there are more additional nucleation sites in the *a*CNC filled systems. This may overwhelm decreased nucleation ability of each CNC particle caused by the surface acetylation, finally leading to the enhanced nucleating efficiency in the *a*CNC filled systems. Besides, the *a*CNC filled systems have higher system rigidity than the pristine CNC filled one (the former has higher modulus than the latter by about one order of magnitude at the identical filler loadings (Xu et al. 2016). This also favors the formation of cellular structure with smaller cell size and narrower size distribution.

Tensile properties of PLA and its nanocomposite foams

However, all nanocomposite foams show poor cell wall structure as compared with the neat PLA one, as can be seen in Fig. 2. At current physical foaming conditions, PLA foam presents good wall structure with uniform wall thickness and smooth wall surface (Fig. 2a). The presence of CNC particles increases the roughness of wall surface and defects remarkably. There are some breakages and cracks on the cell wall surface of nanocomposite foams (see the hollow arrows in Fig. 2b–d), and some free ends of pristine CNC even puncture cell wall, forming defective wall structure (see the solid arrows in Fig. 2b). As discussed above, CNC particles can provide nucleation sites due to their high specific surface area and surface energy. The trapped CO_2 fluid then induces the occurrence of cell nucleation around CNC particles during foaming. The followed CO_2 diffusion promotes bubble growth, generating a strong extension force onto the cell wall (Ji et al. 2013; Ema et al. 2006; Wu et al. 2015). The stress is easily concentrated around the weak polymer-particle interface and big CNC aggregates, resulting in the formation of broken wall structure, especially in the case of decreased wall thickness resulted from increased cell density.

For the pristine CNC filled foam, poor particle-polymer interactions lead to a poor dispersion of CNC particles (confirmed by the SEM and TEM observations reported in the previous work (Xu et al. 2016), and as a result, the cell wall surface is possibly penetrated with free ends of CNC or sharp edges of big CNC aggregates, especially around the phase interface, forming a rough wall surface structure (Fig. 2b). For the *a*CNC filled systems, this trend weakens evidently due to improved polymer-particle affinity. However, the broken level of cell wall surface is enhanced (Fig. 2c, d), which is due to the sharply decreased wall thickness. In other words, the increased expansion ratio caused by the increased nucleation efficiency yields higher extension stress in the systems, resulting in formation of more surface defects during foaming.

The final mechanical properties of those nanocomposite foams are closely related to their microcellular structures, including the cell density and structure, wall thickness and surface defects, as well as the dispersion of nanoparticles, etc. Figure 3 reveals tensile behavior of the neat PLA and its composite foams. It is seen that PLA–CNC foam has lower Young's modulus and tensile strength than the neat PLA one. This is expected. The increased cell density means that there is a higher volume ratio of "hollow" pore phase in this system, and as a result, leads to decreased modulus. While the defective wall surface,

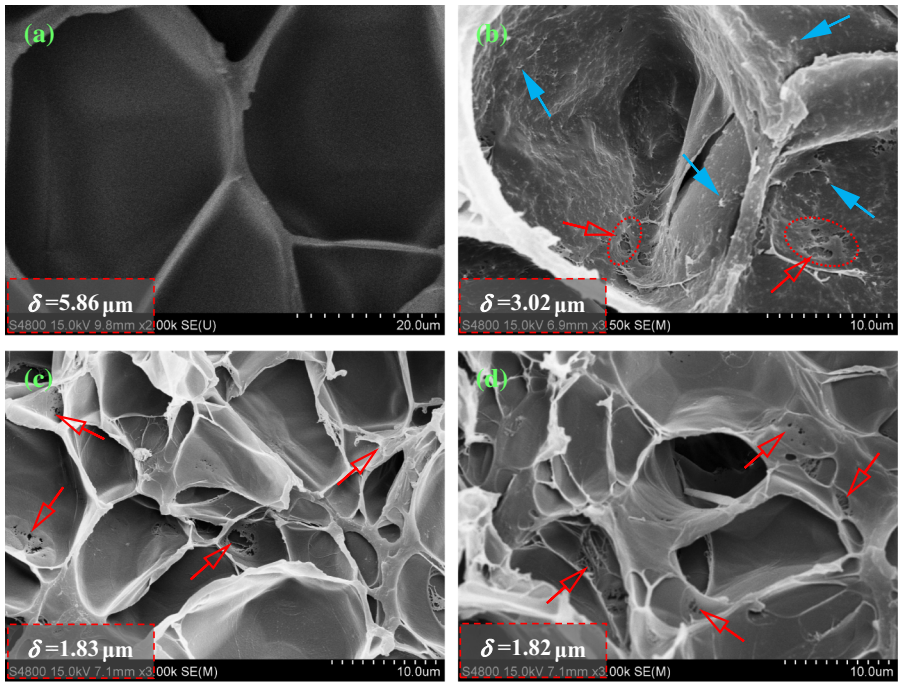

Fig. 2 SEM images for the four kinds of foam samples: **a** PLA, **b** PLA–CNC, **c** PLA-*a*CNC(L) and **d** PLA-*a*CNC(M). The scale bars for (**a**) and for (**b–d**) are 20 μm and 10 μm, respectively

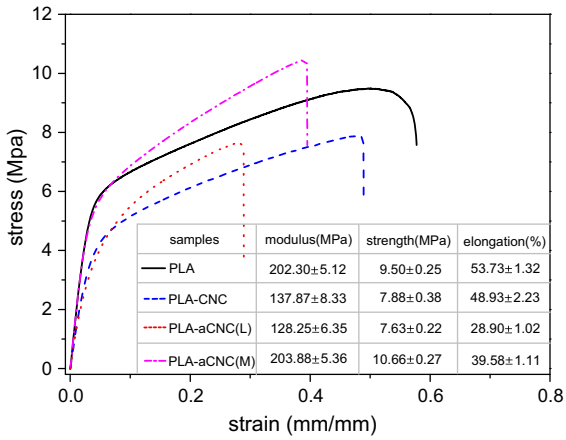

Fig. 3 Tensile curves for the PLA and its composite foams

together with decreased wall thickness, might merely have negative contribution to the strength. PLA–*a*CNC(L) foam shows the same decreased trend with PLA–CNC one. It indicates that the improved level of phase adhesion is not enough to guarantee good load transfer from the matrix to the filled particles in the case of their lower surface DS. In this case, the formation of more surface defects and the decreased wall thickness dominate the overall mechanical properties. However, PLA–*a*CNC(M) foam shows higher strength as compared with the neat PLA one, with almost the identical level of modulus. Relative to the *a*CNC particles with lower DS, those with moderate DS present stronger interactions with matrix polymer [confirmed by the increased value of Flory–Huggins interaction parameter (Xu et al. 2017b)]. The reinforcement of *a*CNC, in this case, can be played to some extent and overwhelms the negative contribution by the increased wall defects and decreased wall thickness. Or at least, the *a*CNC with moderate DS can be used as the heterogeneous agent to control the overall microcellular structure of PLA foams, while maintaining strength level of PLA foams. (the *a*CNC particles with higher DSs are not taken into account here because stronger surface acetylation (DS > 2) destroyed the rigid rod-like structure of CNC particles, making them unsuitable to be used as filler particles any more (Xu et al. 2017b).

Cyclic tensile behavior of PLA and its nanocomposite foams

Clearly, the CNC particles filled PLA nanocomposite foams can be considered as the complex systems with

multi-phases (continuous matrix phase, and dispersed particle and pore phases) and multi-components (PLA, CNC and pore). Here, the tensile cycle tests (with large-scale deformation) were used as the tools to detect the relationships between those structures and nonlinear elastic and plastic deformation behavior of PLA and its nanocomposite foams. Figure 4a shows the strain-controlled cyclic tensile deformation results for four kinds of foam samples. The shapes of these curves are resulted from progressively plastic and elastic deformation of amorphous polymers with higher level of residual strain/stress at zero stress/strain (Deplace et al. 2010; Wang et al. 2010; Hiss et al. 1999). The neat PLA foam has the most cycle numbers among all samples, indicating that it has the highest plasticity at break. This agrees well with its highest elongation level at break shown in Fig. 3.

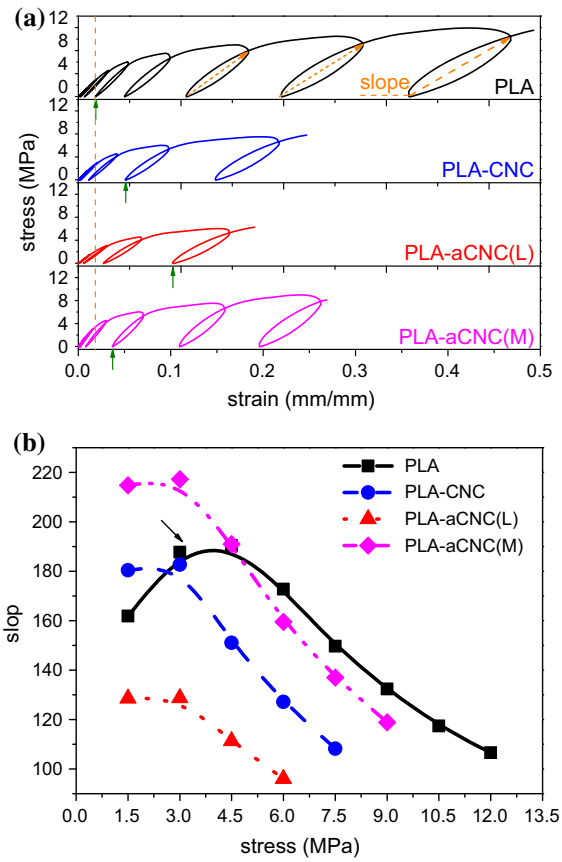

Fig. 4 **a** stress-controlled cyclic tensile deformation for four kinds of foams and **b** as-obtained values of apparent slope of each cycles

At a constant stress level, the deformation (large strain) level can be regarded as a measure of viscoplasticity or viscoelasticity. Taking the fourth cycle as an example, it is seen that PLA–*a*CNC(M) has the lowest strain level among all three nanocomposite foams (see the solid arrows in Fig. 4a), confirming its highest system rigidity. All samples keep deforming during cyclic tests till to be broken. It is a nonlinear process. The slope of the lines connecting starting point of a cycle and terminal point of last one (see the dash arrows in Fig. 4a) can be understood as the "apparent modulus" to describe the first half of a cycle (positive direction of a large scale deformation) at that stress level. The results are summarized in Fig. 4b. It is of interest that the neat PLA foam shows a strain-hardening-like behavior (see the arrow) at the beginning of cyclic deformation, which is not that remarkable on the nanocomposite foams. This is possibly because much more regular and better cellular structure of neat PLA foam is more easily to be orientated along tensile direction or the orientated cellular structure of neat PLA foam is more regular than those of nanocomposite foams, as described schematically in Fig. 5. For the nanocomposite foams, the presence of wall defects easily results in break-down of cell wall during large-scale deformation, and hence, they do not reveal evident strain-hardening-like behavior. As expected, PLA–*a*CNC(M) have higher slope values at the beginning of large-scale deformation because of good reinforcement of the *a*CNC particles with moderate DS. But with the development of deformation, all nanocomposite foams present lower slope values than the neat PLA one. This indicates that the development of cell wall defects (breakages and cracks) begins to dominate the system rigidity with increasing strain level, reducing resistance of foams to deformation.

Clearly, the cycle development is determined by both the plasticity and the elasticity. The strain-controlled cyclic tests may reveal more information about the contribution by these two parts, and the results are given in Fig. 6. The difference in the cycle amounts among the four kinds of foams shows the same trend with that revealed by the stress-controlled tests (Fig. 4a). Generally, for the highly deformable materials, true strains (ε_H) are defined as ln (L/L_0), where L/L_0 is the extension ratio. The true stress $\sigma_t = \sigma_n(L/L_0)$ and ε_H in each cycle can be obtained by experimental tests. According to Strobl's approach

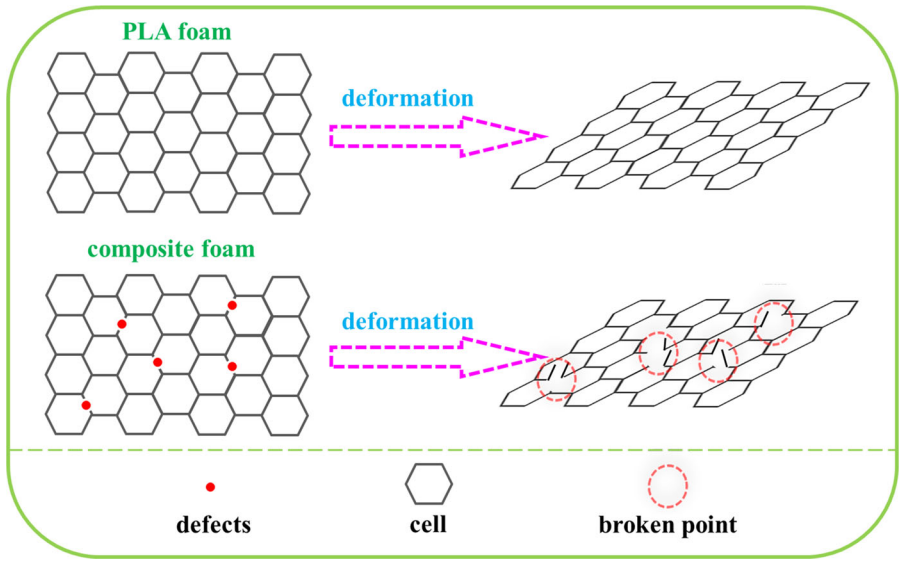

Fig. 5 Diagrams of orientation of microcellular structure of PLA and its composites during stress-controlled cyclic tensile deformation

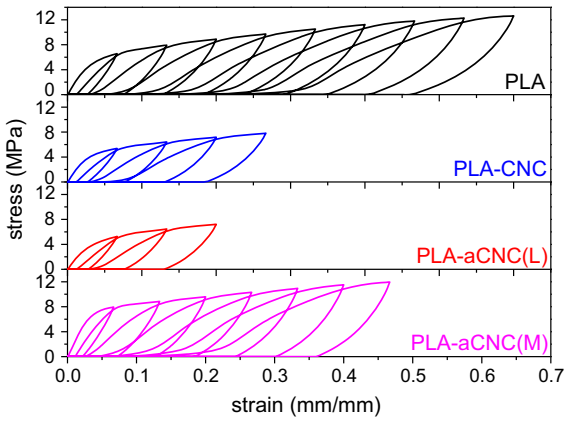

Fig. 6 Strain-controlled cyclic tensile deformation for four kinds of foam samples

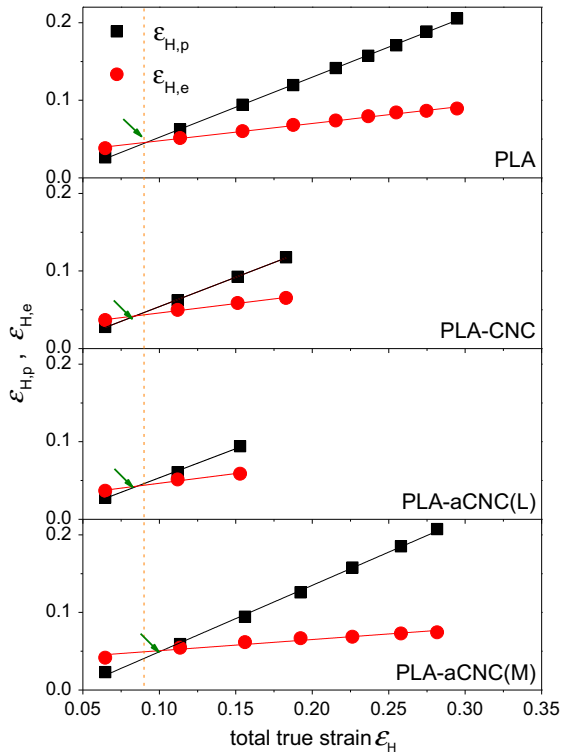

Fig. 7 Plastic and elastic true strains versus the total true strain at the maximum of each cycle of a stress-controlled step cycle tensile test for four kinds of foam samples

(Hiss et al. 1999), the maximum true strain in each cycle as the sum of an elastic component $\varepsilon_{H,e}$ and a plastic component $\varepsilon_{H,p}$ can then be calculated, and the results are shown in Fig. 7. The intersection means a critical point where the phase separation structure begins to be broken down for the multi-phase systems (Huang et al. 2016; Qiu et al. 2016; Chen et al. 2017). For the foams in this work, it is indicative of a beginning of break-down of cellular structure, for instance, collapse of cell wall, breaking or tearing of cell, etc. It can be seen that PLA–CNC and PLA–*a*CNC(L) foams have almost the same location of intersection with that of the neat PLA one. PLA–*a*CNC(M) foam presents an evident upshift of intersection (see the arrow in Fig. 7), however, indicating a decreased plasticity or increased elasticity in this system relative to the neat PLA foam.

Figure 8 gives plastic and elastic true strains of each cycle for those foam samples. It is seen that PLA–CNC and PLA–*a*CNC(L) foams have almost the same levels of both the plastic and elastic true strains with those of neat PLA foam. This does not mean that the presence of CNC particles and as-resulted changes of cellular structure have no influence on the viscoelastic properties. The final performance is determined by the synergistic effects contributed by the increased cell density, reduced thickness of cell wall, and the wall defects (namely the different-level structures of PLA foams) caused by the presence of CNC particles. There is just no clear information because the cycle amounts of these two foams are too small at the current cyclic deformation conditions. For PLA–*a*CNC(M) foam, however, it has higher elasticity at the lower deformation level than the neat PLA one (Fig. 8b), confirming good reinforcement of the *a*CNC particles in this system again. In other words, PLA–*a*CNC(M) foam has higher resistance to the plastic deformation than the neat PLA one at the beginning of deformation (Fig. 8a). At the later stage, however, the elastic strain of this kind of foam decreases remarkably relative to the neat PLA one. In this case, the cell wall defects dominate the following deformation process, resulting in an increased level of plastic strain (as compared with the neat PLA foam) caused by the unrecoverable breaking of defects (Fig. 8b).

The improvement of resistance of PLA–*a*CNC(M) foam to large-scale deformation is further confirmed by the tensile work (calculated by cycle area), as shown in Fig. 9. Taking the third cycle as an example, PLA–*a*CNC(M) foam has the highest tensile work among all samples, indicating a highest energy loss level in this system during a cycle tensile (Huang et al. 2016; Qiu et al. 2016). Additionally, the development of cycle area presents higher slope than that of neat PLA foam, which is also indicative of an

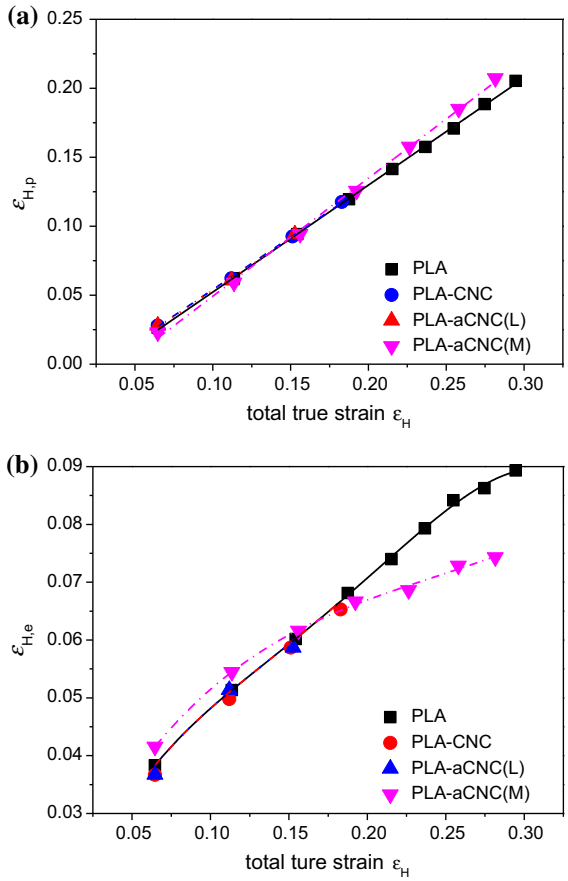

Fig. 8 **a** Plastic and **b** elastic true strains of each cycle of a stress-controlled step cycle tensile test for four kinds of foam samples

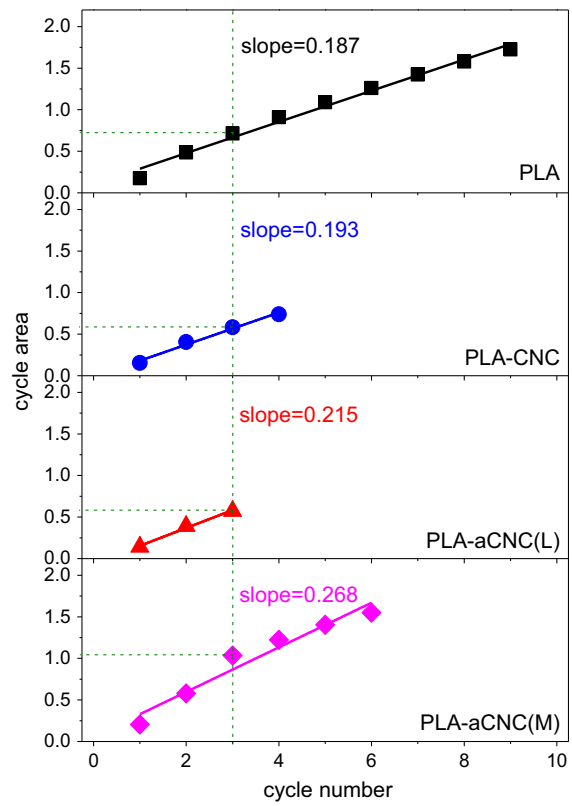

Fig. 9 The development of cycle area of each tensile cycle for four kinds of foam samples during stress-controlled step cycle tensile test

improved system resistance to deformation. Actually, both the PLA–CNC and PLA–*a*CNC(L) foams show higher slope values than the neat PLA one, indicating that both the pristine CNC and the *a*CNC with lower DS have reinforcing effect to some degree. Therefore, the *a*CNC with moderate surface DS are the best one among all three nanoparticles used in this work to achieve the optimal level between enhanced reinforcement of particles and increased surface defects of cell wall, and between improved particle dispersion and decreased wall thickness.

Conclusions

PLA/CNC nanocomposite foams were successfully prepared by batch foaming with high pressure CO_2. The presence of CNC particles results in increase of cell density, with decreased wall thickness, because of the nucleation agent role of those particles during foaming. However, the wall surface defects also increase in this case. The final mechanical properties of those composite foams are determined by a synergistic effect of different cellular structures, including cell density and structure, wall thickness and surface defects, and the dispersion of nanoparticles and their affinity to matrix PLA. For the pristine CNC and the acetylated CNC with lower DS filled composite foams, their tensile strengths and Young's moduli decrease as compared with the neat PLA one because the wall defects and broken cell structure dominate the final mechanical properties of those two systems. For the acetylated CNC particles with moderate DS filled foam, the trend is reversed because the reinforcement of CNC particles to the nanocomposite foam can be shown in the case of highly improved polymer-particle phase adhesion, despite the formation of cell wall defects. The nonlinear deformation behavior during tensile cyclic tests can reveal additional information on the evolution of cell structure during large-scale deformation in the presence of CNC particles. Both the improved phase adhesion and the evolution of wall defects have contributions to the system elasticity and plasticity and these two contributions can be preliminarily distinguished by the tensile strain–stress cycle parameters. Among all three kinds of CNC particles used in this work, the acetylated one with moderate DS is the best one to achieve the optimal level between enhanced reinforcement of nanoparticles and increased surface defects of cell wall.

Acknowledgments Financial support from the National Natural Science Foundation of China (51573156) is gratefully acknowledged.

References

Alvarado N, Romero J, Torres A, López de Dicastillo C, Rojas A, Galotto MJ, Guarda A (2018) Supercritical impregnation of thymol in poly(lactic acid) filled with electrospun poly(vinyl alcohol)-cellulose nanocrystals nanofibers: development an active food packaging material. J Food Eng 217:1–10

Arrieta MP, Fortunati E, Dominici F, Rayon E, Lopez J, Kenny JM (2014) Multifunctional PLA–PHB/cellulose nanocrystal films: processing, structural and thermal properties. Carbohydr Polym 107:16–24

Arrieta MP, Fortunati E, Dominici F, Lopez J, Kenny JM (2015) Bionanocomposite films based on plasticized PLA–PHB/cellulose nanocrystal blends. Carbohydr Polym 121:265–275

Bitinis N, Fortunati E, Verdejo R, Bras J, Kenny JM, Torre L, Lopez-Manchado MA (2013a) Poly(lactic acid)/natural rubber/cellulose nanocrystal bionanocomposites Part II: properties evaluation. Carbohydr Polym 96(2):621–627

Bitinis N, Verdejo R, Bras J, Fortunati E, Kenny JM, Torre L, Lopez-Manchado MA (2013b) Poly(lactic acid)/natural rubber/cellulose nanocrystal bionanocomposites part I: processing and morphology. Carbohydr Polym 96(2):611–620

Borkotoky SS, Dhar P, Katiyar V (2017) Biodegradable poly (lactic acid)/cellulose nanocrystals (CNCs) composite microcellular foam: effect of nanofillers on foam cellular morphology, thermal and wettability behavior. Int J Biol Macromol. https://doi.org/10.1016/j.ijbiomac.2017.08.036

Cacciotti I, Fortunati E, Puglia D, Kenny JM, Nanni F (2014) Effect of silver nanoparticles and cellulose nanocrystals on electrospun poly(lactic) acid mats: morphology, thermal properties and mechanical behavior. Carbohydr Polym 103:22–31

Chen J, Xu C, Wu D, Pan K, Qian A, Sha Y, Wang L, Tong W (2015) Insights into the nucleation role of cellulose crystals during crystallization of poly(beta-hydroxybutyrate). Carbohydr Polym 134:508–515

Chen JX, Wang YK, Yin ZR, Tam KC, Wu DF (2017) Morphology and mechanical properties of poly(beta-hydroxybutyrate)/poly(epsilon-caprolactone) blends controlled with cellulosic particles. Carbohydr Polym 174:217–225

Cho SY, Park HH, Yun YS, Jin H-J (2012) Influence of cellulose nanofibers on the morphology and physical properties of poly(lactic acid) foaming by supercritical carbon dioxide. Macromol Res 21(5):529–533

Deplace F, Wang Z, Lynd NA, Hotta A, Rose JM, Hustad PD, Tian J, Ohtaki H, Coates GW, Shimizu F, Hirokane K, Yamada F, Shin Y-W, Rong L, Zhu J, Toki S, Hsiao BS, Fredrickson GH, Kramer EJ (2010) Processing–structure–

mechanical property relationships of semicrystalline polyolefin-based block copolymers. J Polym Sci Part B Polym Phys 48(13):1428–1437

Dhar P, Bhasney SM, Kumar A, Katiyar V (2016) Acid functionalized cellulose nanocrystals and its effect on mechanical, thermal, crystallization and surfaces properties of poly (lactic acid) bionanocomposites films: a comprehensive study. Polymer 101:75–92

Dhar P, Gaur SS, Soundararajan N, Gupta A, Bhasney SM, Milli M, Kumar A, Katiyar V (2017) Reactive extrusion of polylactic acid/cellulose nanocrystal films for food packaging applications: influence of filler type on thermomechanical, rheological, and barrier properties. Ind Eng Chem Res 56(16):4718–4735

Dlouhá J, Suryanegara L, Yano H (2012) The role of cellulose nanofibres in supercritical foaming of polylactic acid and their effect on the foam morphology. Soft Matter 8(33):8704

Dong F, Yan M, Jin C, Li S (2017) Characterization of type-II acetylated cellulose nanocrystals with various degree of substitution and its compatibility in PLA films. Polymers 9(8):346

Ema Y, Ikeya M, Okamoto M (2006) Foam processing and cellular structure of polylactide-based nanocomposites. Polymer 47(15):5350–5359

Fang HG, Zhang YQ, Bai J, Wang ZK, Wang ZG (2013) Bimodal architecture and rheological and foaming properties for gamma-irradiated long-chain branched polylactides. RSC Adv 3:8783–8795

Fortunati E, Armentano I, Zhou Q, Iannoni A, Saino E, Visai L, Berglund LA, Kenny JM (2012a) Multifunctional bionanocomposite films of poly(lactic acid) cellulose nanocrystals and silver nanoparticles. Carbohydr Polym 87(2):1596–1605

Fortunati E, Peltzer M, Armentano I, Torre L, Jiménez A, Kenny JM (2012b) Effects of modified cellulose nanocrystals on the barrier and migration properties of PLA nano-biocomposites. Carbohyd Polym 90(2):948–956

Fortunati E, Peltzer M, Armentano I, Jiménez A, Kenny JM (2013) Combined effects of cellulose nanocrystals and silver nanoparticles on the barrier and migration properties of PLA nano-biocomposites. J Food Eng 118:117–124

Fortunati E, Luzi F, Puglia D, Dominici F, Santulli C, Kenny JM, Torre L (2014) Investigation of thermo-mechanical, chemical and degradative properties of PLA-limonene films reinforced with cellulose nanocrystals extracted from Phormium tenax leaves. Eur Polym J 56:77–91

Fortunati E, Luzi F, Puglia D, Petrucci R, Kenny JM, Torre L (2015) Processing of PLA nanocomposites with cellulose nanocrystals extracted from Posidonia oceanica waste: innovative reuse of coastal plant. Ind Crops Prod 67:439–447

Haque MM-U, Puglia D, Fortunati E, Pracella M (2017) Effect of reactive functionalization on properties and degradability of poly(lactic acid)/poly(vinyl acetate) nanocomposites with cellulose nanocrystals. React Funct Polym 110:1–9

Herrera N, Salaberria AM, Mathew AP, Oksman K (2016) Plasticized polylactic acid nanocomposite films with cellulose and chitin nanocrystals prepared using extrusion and compression molding with two cooling rates: effects on mechanical, thermal and optical properties. Compos A Appl Sci Manuf 83:89–97

Hiss R, Hobeika S, Lynn C, Strobl G (1999) Network stretching, slip processes, and fragmentation of crystallites during uniaxial drawing of polyethylene and related copolymers. A comparative study. Macromolecules 32:4390–4403

Huang J, Wang J, Qiu YX, Wu DF (2016) Mechanical properties of thermoplastic polyester elastomer controlled by blending with poly(butylene terephthalate). Polym Test 55:152–159

Ji GY, Zhai WT, Lin DP, Ren Q, Zheng WG, Jung DW (2013) Microcellular foaming of poly(lactic acid)/silica nanocomposites in compressed CO_2: critical influence of crystallite size on cell morphology and foam expansion. Ind Eng Chem Res 52(19):6390–6398

Kang DJ, Xu D, Zhang ZX, Pal K, Bang DS, Kim JK (2009) Well-controlled microcellular biodegradable PLA/silk composite foams using supercritical CO_2. Macromol Mater Eng 294(9):620–624

Keshtkar M, Nofar M, Park CB, Carreau PJ (2014) Extruded PLA/clay nanocomposite foams blown with supercritical CO_2. Polymer 55(16):4077–4090

Khoshkava V, Kamal MR (2014) Effect of cellulose nanocrystals (CNC) Particle morphology on dispersion and rheological and mechanical properties of polypropylene/CNC nanocomposites. ACS Appl Mater Interfaces 6(11):8146–8157

Li S, Deng L, Xu C, Wu QH, Wang ZG (2017) Making a supertough flame-retardant polylactide composite through reactive blending with ethylene–acrylic ester–glycidyl methacrylate terpolymer and addition of aluminum hypophosphite. ACS Omega 2:1886–1895

Liao X, Nawaby AV, Whitfield PS (2010) Carbon dioxide-induced crystallization in poly(*L*-lactic acid) and its effect on foam morphologies. Polym Int 59(12):1709–1718

Lin N, Huang J, Chang PR, Feng J, Yu J (2011) Surface acetylation of cellulose nanocrystal and its reinforcing function in poly(lactic acid). Carbohydr Polym 83(4):1834–1842

Luzi F, Fortunati E, Puglia D, Petrucci R, Kenny JM, Torre L (2015) Study of disintegrability in compost and enzymatic degradation of PLA and PLA nanocomposites reinforced with cellulose nanocrystals extracted from Posidonia Oceanica. Polym Degrad Stab 121:105–115

Luzi F, Fortunati E, Jiménez A, Puglia D, Pezzolla D, Gigliotti G, Kenny JM, Chiralt A, Torre L (2016) Production and characterization of PLA–PBS biodegradable blends reinforced with cellulose nanocrystals extracted from hemp fibres. Ind Crops Prod 93:276–289

Lv QL, Xu CJ, Wu DF, Wang ZF, Lan RY, Wu LS (2017) The role of nanocrystalline cellulose during crystallization of poly(ε-caprolactone) composites: nucleation agent or not? Compos A Appl Sci Manuf 92:17–26

Matuana LM (2008) Solid state microcellular foamed poly(lactic acid): morphology and property characterization. Bioresour Technol 99:3643–3650

Matuana LM, Faruk O (2010) Effect of gas saturation conditions on the expansion ratio of microcellular poly(lactic acid)/-wood-flour composites. eXPRESS. Polym Lett 4(10):621–631

Miao C, Hamad WY (2013) Cellulose reinforced polymer composites and nanocomposites: a critical review. Cellulose 20(5):2221–2262

Nam P, Maiti P, Okamoto M, Koaka T (2002) Foam processing and cellular structure of polypropylene/clay nanocomposites. Polym Eng Sci 42(9):1907–1918

Nofar M, Park CB (2014) Poly (lactic acid) foaming. Prog Polym Sci 39(10):1721–1741

Pal N, Dubey P, Gopinath P, Pal K (2017) Combined effect of cellulose nanocrystal and reduced graphene oxide into poly-lactic acid matrix nanocomposite as a scaffold and its anti-bacterial activity. Int J Biol Macromol 95:94–105

Parize D, Oliveira JE, Williams T, Wood D, Avena-Bustillos RJ, Klamczynski AP, Glenn GM, Marconcini JM, Mattoso LHC (2017) Solution blow spun nanocomposites of poly(lactic acid)/cellulose nanocrystals from Eucalyptus kraft pulp. Carbohydr Polym 174:923–932

Pracella M, Haque MM-U, Puglia D (2014) Morphology and properties tuning of PLA/cellulose nanocrystals bio-nanocomposites by means of reactive functionalization and blending with PVAc. Polymer 55(16):3720–3728

Qiu YX, Wang J, Wu DF, Wang ZF, Zhang M, Yao Y, Wei NX (2016) Thermoplastic polyester elastomer nanocomposites filled with graphene: mechanical and viscoelastic properties. Compos Sci Technol 132:108–115

Raquez J-M, Habibi Y, Murariu M, Dubois P (2013) Polylactide (PLA)-based nanocomposites. Prog Polym Sci 38(10–11):1504–1542

Salmieri S, Islam F, Khan RA, Hossain FM, Ibrahim HMM, Miao C, Hamad WY, Lacroix M (2014) Antimicrobial nanocomposite films made of poly(lactic acid)-cellulose nanocrystals (PLA–CNC) in food applications-part B: effect of oregano essential oil release on the inactivation of Listeria monocytogenes in mixed vegetables. Cellulose 21(6):4271–4285

Shi Q, Zhou C, Yue Y, Guo W, Wu W, Wu Q (2012) Mechanical properties and in vitro degradation of electrospun bio-nanocomposite mats from PLA and cellulose nanocrystals. Carbohydr Polym 90:301–308

Spinella S, Lo Re G, Liu B, Dorgan J, Habibi Y, Leclèr P, Raquez J-M, Dubois P, Gross RA (2015) Polylactide/cellulose nanocrystal nanocomposites: efficient routes for nanofiber modification and effects of nanofiber chemistry on PLA reinforcement. Polymer 65:9–17

Wang Z, Niu Y, Fredrickson G, Kramer E, Shin Y, Shimizu F, Zuo F, Rong L, Hsiao BS, Coates GW (2010) Step-cycle mechanical processing of gels of *s*PP-*b*-EPR-*b*-*s*PP triblock copolymer in mineral oil. Macromolecules 43(16):6782–6788

Wang XX, Kumar V, Li W (2012) Development of crystallization in PLA during solid-state foaming process using sub-critical CO_2. Cell Polym 31(1):1–18

Wu DF, Lv QL, Feng SH, Chen J, Chen YX, Qiu YX, Yao X (2015) Polylactide composite foams containing carbon nanotubes and carbon black: synergistic effect of filler on electrical conductivity. Carbon 95:380–387

Xin TT, Yuan T, Xiao S, He J (2011) Synthesis of cellulose-*graft*-poly(methyl methacrylate) via homogeneous ATRP. BioResources 92:17–26

Xu HJ, Fang HG, Bai J, Zhang YQ, Wang ZG (2014) Preparation and characterization of high-melt-strength polylactide with long-chain branched structure through γ-radiation-induced chemical reactions. Ind Eng Chem Res 53:1150–1159

Xu CJ, Chen J, Wu DF, Chen YX, Lv QL, Wang M (2016) Polylactide/acetylated nanocrystalline cellulose composites prepared by a continuous route: a phase interface-property relation study. Carbohydr Polym 146:58–66

Xu CJ, Lv QL, Wu DF, Wang ZF (2017a) Polylactide/cellulose nanocrystal composites: a comparative study on cold and melt crystallization. Cellulose 24:2163–2175

Xu CJ, Wu DF, Lv QL, Yan L (2017b) Crystallization temperature as the probe to detect polymer-filler compatibility in the poly(ε-caprolactone) composites with acetylated cellulose nanocrystal. J Phys Chem C 121(34):18615–18624

Yu HY, Yang XY, Lu FF, Chen GY, Yao JM (2016) Fabrication of multifunctional cellulose nanocrystals/poly(lactic acid) nanocomposites with silver nanoparticles by spraying method. Carbohydr Polym 140:209–219

Zhang AJ, Zhang QK, Bai H, Li L, Li J (2014) Polymeric nanoporous materials fabricated with supercritical CO_2 and CO_2-expanded liquids. Chem Soc Rev 43(20):6938–6953

Zhang C, Salick MR, Cordie TM, Ellingham T, Dan Y, Turng LS (2015) Incorporation of poly(ethylene glycol) grafted cellulose nanocrystals in poly(lactic acid) electrospun nanocomposite fibers as potential scaffolds for bone tissue engineering. Mater Sci Eng C Mater Biol Appl 49:463–471

Zhao J, Zhao Y, Wang Z, Peng Z (2016) Effect of polymorphs of cellulose nanocrystal on the thermal properties of poly(lactic acid)/cellulose nanocrystal composites. Eur Phys J E Soft Matter 39(12):118

Zhou CJ, Shi QF, Guo WH, Terrell L, Qureshi AT, Hayes DJ, Wu QL (2013) Electrospun bio-nanocomposite scaffolds for bone tissue engineering by cellulose nanocrystals reinforcing maleic anhydride grafted PLA. ACS Appl Mater Interfaces 5(9):3847–3854